Polarization control of single photon quantum orbital angular momentum states

E. Nagali,[1] F. Sciarrino,[1,*] F. De Martini,[1,2] B. Piccirillo,[3,4] E. Karimi,[3,5] L. Marrucci,[3,5] and E. Santamato[3,4]

[1] *Dipartimento di Fisica dell'Università "La Sapienza" and Consorzio Nazionale Interuniversitario per le Scienze Fisiche della Materia, Roma 00185, Italy*
[2] *Accademia Nazionale dei Lincei, via della Lungara 10, Roma 00165, Italy*
[3] *Dipartimento di Scienze Fisiche, Università di Napoli "Federico II", Compl. Univ. di Monte S. Angelo, 80126 Napoli, Italy*
[4] *Consorzio Nazionale Interuniversitario per le Scienze Fisiche della Materia, Napoli*
[5] *CNR-INFM Coherentia, Compl. Univ. di Monte S. Angelo, 80126 Napoli, Italy*

(Dated: December 15, 2008)

The orbital angular momentum of photons, being defined in an infinitely dimensional discrete Hilbert space, offers a promising resource for high-dimensional quantum information protocols in quantum optics. The biggest obstacle to its wider use is presently represented by the limited set of tools available for its control and manipulation. Here, we introduce and test experimentally a series of simple optical schemes for the coherent transfer of quantum information from the polarization to the orbital angular momentum of single photons and vice versa. All our schemes exploit a newly developed optical device, the so-called "q-plate", which enables the manipulation of the photon orbital angular momentum driven by the polarization degree of freedom. By stacking several q-plates in a suitable sequence, one can also access to higher-order angular momentum subspaces. In particular, we demonstrate the control of the orbital angular momentum m degree of freedom within the subspaces of $|m| = 2\hbar$ and $|m| = 4\hbar$ per photon. Our experiments prove that these schemes are reliable, efficient and have a high fidelity.

arXiv:0902.0740v1 [quant-ph] 4 Feb 2009

INTRODUCTION

Quantum information is based on the combination of classical information theory and quantum mechanics. In the last few decades, the development of this new field has opened far-reaching prospects both for fundamental physics, such as the capability of a full coherent control of quantum systems, as well as in technological applications, most significantly in the communication field. In particular, quantum optics has enabled the implementation of a variety of quantum-information protocols. However, in this context, the standard information encoding based on the two-dimensional quantum space of photon polarizations (or "spin" angular momentum) imposes significant limitations to the protocols that may be implemented. To overcome such limitations, in recent years the orbital angular momentum (OAM) of light, related to the photon's spatial mode structure, has been recognized as a new powerful resource for novel quantum information protocols, allowing the implementation with a single photon of a higher-dimensional quantum space, or a "qudit" [1, 2]. Thus far, the generation of OAM-entangled photon pairs has been carried out by exploiting the process of parametric down-conversion [3, 4, 5, 6, 7] and the quantum state tomography of such entangled states has been achieved by using holographic masks [8] and single mode fibers [9]. The observation of pairs of photons simultaneously entangled in polarization and OAM has been also reported and exploited for quantum information protocols [10, 11, 12, 13].

Despite these successes, the optical tools for controlling the OAM quantum states have been rather limited: the possibility of a wider control and manipulation of the OAM resource, analogous to that currently possible for the polarization degree of freedom, is yet to be achieved.

As we demonstrate here, these limitations can be overcome by exploiting the properties of an optical device, named "q-plate", which has been recently introduced both in the classical and in the quantum domain [14, 15]. The main feature of the q-plate is its capability of coupling the spinorial (polarization) and orbital contributions of the angular momentum of photons. The ease of use, flexibility and good conversion efficiency showed by this device makes it a promising tool for exploiting the OAM degree of freedom of photons, in combination with polarization, as a resource to implement high-dimensional quantum information protocols. In our previous work [15] we provided a first demonstration of the coherent information transfer capabilities for the simplest optical schemes based on the q-plate, and for the case of a two-photon state with non-classical correlations. In this paper we restrict our attention to the single photon case and demonstrate, by quantum tomography, the good coherence and fidelity of the information transfer and the possibility to encode and then decode the information within the orbital angular momentum space of a single photon [16]. This last experiment is equivalent to a demonstration of quantum communication taking place entirely in the orbital angular momentum alphabet, with an overall efficiency that is in principle much higher than previously demonstrated. Finally, we demonstrate the transfer of quantum information to a higher order angular momentum subspace by stacking more q-plates in sequence.

This paper is organized as follows. In Section II we illustrate the q-plate device and its properties in the sin-

gle photon regime. A description of the different optical schemes adopted and of the experimental setup is given in Section III. As mentioned above, we have worked in the OAM SU(2) subspace $|m| = 2$ (we will denote it as o_2) and in the subspace $|m| = 4$ (or o_4), where m will hereafter denote the quantum number giving the OAM per photon along the beam axis in units of $\hbar$. Details on the hologram devices used for the quantum tomography of photons in these OAM subspaces are given in Sec. IV. The demonstration of quantum information transfer from the polarization quantum space to the OAM o_2 subspace and *vice versa* is given in Sec. V, while Sec. VI is concerned about the o_4 subspace. A brief conclusion is given in Sec. VII.

THE Q-PLATE

A q-plate (QP) is a birefringent slab having a suitably patterned transverse optical axis, with a topological singularity at its center [14]. The "charge" of this singularity is given by an integer or half-integer number q, which is determined by the (fixed) pattern of the optical axis. The birefringent retardation δ must instead be uniform across the device. Q-plates working in the visible or near-infrared domain can be manufactured with nematic liquid crystals, by means of a suitable treatment of the containing substrates [14, 17]. Once a liquid crystal QP is assembled, the birefringent retardation δ can be tuned either by mechanical compression (exploiting the elasticity of the spacers that fix the thickness of the liquid crystal cell) or by temperature control.

For $\delta = \pi$, a QP modifies the OAM state m of a light beam crossing it, imposing a variation $\Delta m = \pm 2q$ whose sign depends on the input polarization, positive for left-circular and negative for right-circular [18]. The handedness of the output circular polarization is also inverted, i.e. the optical spin is flipped [19]. In the present work, we use only QPs with charge $q = 1$ and $\delta \simeq \pi$. Hence, an input TEM_{00} mode (having $m = 0$) is converted into a beam with $m = \pm 2$, as illustrated pictorially in Fig. 1. In a single-photon quantum formalism, the QP implements the following quantum transformations on the single photon state:

$$\begin{aligned} |L\rangle_\pi |m\rangle_o &\rightarrow |R\rangle_\pi |m+2\rangle_o \\ |R\rangle_\pi |m\rangle_o &\rightarrow |L\rangle_\pi |m-2\rangle_o \end{aligned} \qquad (1)$$

where $|\cdot\rangle_\pi$ and $|\cdot\rangle_o$ stand for the photon quantum state 'kets' in the polarization and OAM degrees of freedom, and L and R denote the left and right circular polarization states, respectively. In the following, whenever there is no risk of ambiguity, the subscripts π and o will be omitted for brevity.

Any coherent superposition of the two input states given in Eq. (1) is expected to be preserved by the QP transformation, leading to the equivalent superposition of the corresponding output states [15]. Explicitly, we have

$$\alpha|L\rangle_\pi|m\rangle_o + \beta|R\rangle_\pi|m\rangle_o \rightarrow \alpha|R\rangle_\pi|m+2\rangle_o + \beta|L\rangle_\pi|m-2\rangle_o \qquad (2)$$

Finally, we note that the quantum number m does not completely define the transverse mode of the photon. A radial number is also necessary for spanning a complete basis, such as that of the Laguerre-Gauss modes or an equivalent one. This radial degree of freedom however does not play a significant role in the demonstrations that will be reported in the following, because the QP gives rise to a well defined radial profile, independent of the sign of m (see [20]), so for brevity in the following we will omit it from our notations. This radial degree of freedom may however become more critical when states having different values of $|m|$ are manipulated simultaneously, a task which will be addressed in a future paper. However we note that also holograms create modes whose radial profiles are independent of the vortex sign [21]. Such effect shows that our measurements are independent of radial index number.

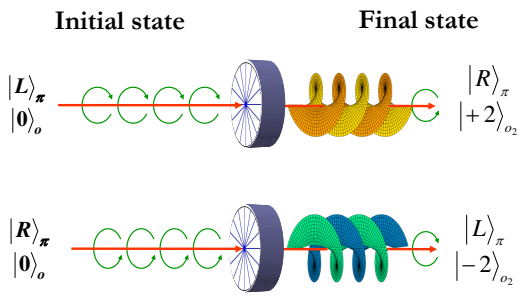

FIG. 1: Pictorial representation of the q-plate device action on a photon quantum state.

EXPERIMENTAL SETUP

Let us now describe the overall scheme of the experimental apparatus, also shown in Fig. 2. The setup can be divided in two main sections. The first one is common to all our experiments and corresponds to the generator of triggered one-photon states, with arbitrary polarization and fixed spatial mode TEM_{00}. The second section is different for the four different experiments (denoted as **a**, **b**, **c**, **d**) that will be described in the following Sections, and is concerned with the OAM and polarization manipulations and with the final quantum-state tomography.

In the first section of the apparatus, the main optical source is a Ti:Sa mode-locked laser, with wavelength $\lambda = 795$ nm, pulse duration of 180 fs, and repetition rate 76 MHz. By second harmonic generation, the output of

the laser is converted into a ultraviolet (UV) beam with wavelength $\lambda_p = 397.5$ nm, which is used as pump beam for the photon pairs generation. The residual field at λ is eliminated by means of a set of dichroic mirrors and filters. The UV beam, with an average power of 600 mW, pumps a 1.5 mm thick nonlinear crystal of β-barium borate (BBO) cut for type II phase-matching, working in a collinear regime and generating polarization pairs of photons with the same wavelength λ and orthogonal linear polarizations, hereafter denoted as horizontal (H) and vertical (V). These down-converted photons are then spatially separated from the fundamental UV beam by a dichroic mirror. The spatial and temporal walk-offs are compensated by a half-wave plate and a 0.75 mm thick BBO (C) [22]. Finally, the photons are spectrally filtered by an interference filter with bandwidth $\Delta\lambda = 6$ nm.

In order to work in the one-photon regime, a polarizing beam-splitter (PBS) transmits the horizontally-polarized photon of the pair and reflects the vertically-polarized one. The latter is then coupled to a single-mode fiber and revealed with a single-photon counter (SPCM), which therefore acts as a trigger of the one-photon state generation. The transmitted photon in the $|H\rangle$ polarization state is coupled to another single-mode fiber, which selects only a pure TEM_{00} transverse mode, corresponding to OAM $m = 0$. The coincidence count rate of the two outputs of the PBS, after coupling into the fibers, is of typically 16-18 kHz.

After the fiber output, two waveplates compensate (C) the polarization rotation introduced by the fiber. Then, a polarizing beam-splitter and a set of wave plates are used for setting the photon polarization to an arbitrary qubit state $|\varphi\rangle_\pi$. This concludes the first section of the apparatus. The one-photon quantum state at this point can be represented by the ket $|\varphi\rangle_\pi|0\rangle_o$.

Let us now consider the second main section of the apparatus. As we mentioned above, this has been mounted in four different configurations, shown in Fig. 2, corresponding to the implementations of the following devices:

a) Quantum transferrer from polarization to OAM subspace $|m| = 2$, i.e. $\pi \to o_2$

b) Quantum transferrer from OAM subspace $|m| = 2$ to polarization, i.e. $o_2 \to \pi$

c) Quantum bidirectional transfer polarization-OAM-polarization, i.e. $\pi \to o_2 \to \pi$

d) Quantum transferrer from polarization to OAM subspace $|m| = 4$, i.e. $\pi \to o_4$

Each process of quantum information transfer is based on a q-plate (two in the cases c and d) combined with other standard polarizers and waveplates. The OAM state is prepared or analyzed by means of suitably-developed holograms, as discussed in the next Section, preceded or followed by coupling to single-mode fibers, which selects the $m = 0$ state $|0\rangle_o$ before detection. After the analysis, the signals have been detected by single photon counters SPCM and then sent to a coincidence box interfaced with a computer, for detecting and counting the coincidences of the photons and the trigger D_T.

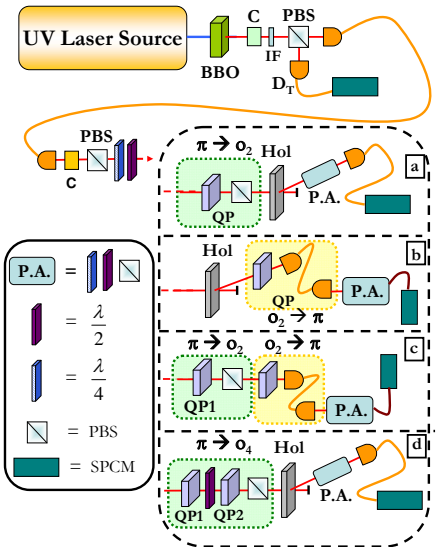

FIG. 2: Schematic representation of the experimental setup. Outside the dashed box is the first section of the apparatus, common to all our experiments. In the dashed box, the four configurations **a, b, c, d** of the second section of the apparatus are shown, used in the four experiments discussed in this paper. Legend: BBO - β-barium borate crystal used for photon-pair generation; C - walk-off compensation stage; PBS - polarizing beam-splitter; D_T trigger detection unit; QP - q-plate; Hol - hologram; S.P.C.M. - Single photon counter module; P.A. - polarization analysis set, as shown in solid-line box.

HOLOGRAMS AND OAM-POLARIZATION CORRESPONDENCE

A full analogy can be drawn between the polarization SU(2) Hilbert space and each subspace of OAM with a given $|m|$, except of course for $m = 0$. This analogy is for example useful for retracing the quantum tomography procedure to the standard one for polarization [9, 23]. In particular, it is convenient to consider the eigenstates of OAM $|\pm|m|\rangle$ as the analog of the circular polarizations $|L\rangle$ and $|R\rangle$, as the latter ones are obviously the eigenstates of the spin angular momentum. To make the analogy more apparent, small-letter symbols $|l\rangle = |+|m|\rangle$ and $|r\rangle = |-|m|\rangle$ are introduced to refer to the OAM case, while the capital letters are used for the polarization. Following the same convention, the OAM equivalent of

the two basis linear polarizations $|H\rangle$ and $|V\rangle$ are then defined as

$$\begin{aligned} |h\rangle &= \frac{1}{\sqrt{2}}(|l\rangle + |r\rangle) \\ |v\rangle &= \frac{1}{i\sqrt{2}}(|l\rangle - |r\rangle) \end{aligned} \tag{3}$$

Finally, the $\pm 45°$ angle "anti-diagonal" and "diagonal" linear polarizations will be hereafter denoted with the kets $|A\rangle = (|H\rangle + |V\rangle)/\sqrt{2}$ and $|D\rangle = (|H\rangle - |V\rangle)/\sqrt{2}$, and the corresponding OAM states are defined analogously:

$$\begin{aligned} |a\rangle &= \frac{1}{\sqrt{2}}(|h\rangle + |v\rangle) = \frac{e^{-i\pi/4}}{\sqrt{2}}(|l\rangle + i|r\rangle) \\ |d\rangle &= \frac{1}{\sqrt{2}}(|h\rangle - |v\rangle) = \frac{e^{i\pi/4}}{\sqrt{2}}(|l\rangle - i|r\rangle). \end{aligned} \tag{4}$$

The holograms used for generating or analyzing the above OAM states were manufactured from a computer-generated image by a photographic technique followed by a chemical bleaching step, producing pure phase binary holographic optical elements. The typical first-order diffraction efficiencies of these holograms were in the range 10-15%. The patterns we used are shown in Fig. 3. Analogously to polarizers, these holograms are used in two ways: (i) for generating a given input quantum state of OAM; (ii) for analyzing a given OAM component of an arbitrary input quantum state.

When using the holograms for generating one of the above OAM states, a TEM_{00} input mode is sent into the hologram and the first-order diffracted mode is used for output. The input beam must be precisely centered on the hologram pattern center. The output OAM quantum state obtained is shown in the upper corner of each hologram pattern in Fig. 3.

When using the holograms for analysis, the input mode, having unknown OAM quantum state, is sent through the hologram (with proper centering). The first-order diffracted output is then coupled to a single-mode fiber, which filters only the $m = 0$ state, before detection. It can be shown that the amplitude of this output is then just proportional to the projection of the input state onto the OAM state shown in the upper corner of each hologram pattern, in Fig. 3 (except, possibly, for a sign inversion of m in the case of the upper row holograms).

MANIPULATION OF ORBITAL ANGULAR MOMENTUM IN THE SUBSPACE $|m| = 2$

A single q-plate (with $q = 1$) can be used for coupling the polarization subspace π with the OAM subspace o_2, spanned by the OAM eigenstates $\{|+2\rangle_o, |-2\rangle_o\}$. In this Section, we present two optical schemes based on the q-plate that enable a qubit of quantum information to be transferred from the polarization to the OAM (setup **a**, *transferrer* $\pi \rightarrow o_2$), from OAM to polarization (setup **b**, *transferrer* $o_2 \rightarrow \pi$). Moreover, we tested also the combination of these two schemes, thus realizing the *bidirectional transfer* polarization-OAM-polarization (setup **c**, $\pi \rightarrow o_2 \rightarrow \pi$). The latter demonstration is equivalent to demonstrating quantum communication using OAM for encoding the message. In other words, the qubit is initially prepared in the polarization space, then passed to OAM in a transmitting unit (Alice), sent to a receiving unit (Bob), where it is transferred back to polarization for further processing or detection.

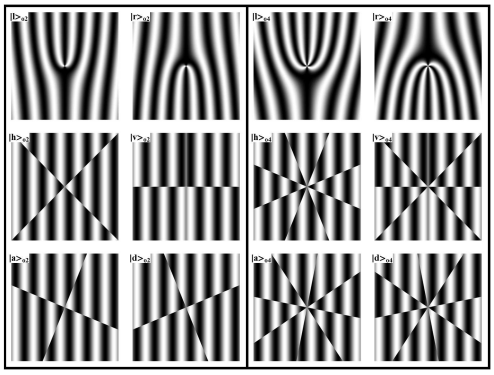

FIG. 3: Patterns of the 12 binary holograms used in this work. The left box refers to the OAM subspace o_2 ($|m| = 2$). The right box to the OAM subspace o_4 ($|m| = 4$). In the upper-left corner of each hologram is shown the quantum state that is generated by the hologram, when using a TEM_{00} input, in the first-order diffraction beam.

All these transfer processes have been experimentally verified by carrying out quantum tomography measurements, either in the polarization or in the OAM degree of freedom. The latter was based on the polarization - OAM subspace analogy discussed in the previous Section. Let us now see the details of each of the three schemes.

Transferrer polarization to OAM

Let us consider as initial state the polarization-encoded qubit

$$|\Psi\rangle_{\mathrm{in}} = |\varphi\rangle_\pi |0\rangle_o = (\alpha|H\rangle_\pi + \beta|V\rangle_\pi)|0\rangle_o \tag{5}$$

where $|0\rangle_o$ indicates the TEM_{00} mode. By passing it through a pair of suitably oriented quarter-waveplates (one with the optical axis parallel to the horizontal direction and the other at 45°), the photon state is rotated into the L, R basis:

$$(\alpha|L\rangle_\pi + \beta|R\rangle_\pi)|0\rangle_o \tag{6}$$

After the QP the quantum state of the photon is then turned into the following:

$$\alpha|R\rangle|+2\rangle+\beta|L\rangle|-2\rangle. \quad (7)$$

If a polarizer along the horizontal direction is used, we then obtain the state

$$|\Psi\rangle_{out}=|H\rangle_\pi(\alpha|+2\rangle_o+\beta|-2\rangle_o)=|H\rangle_\pi|\varphi\rangle_{o_2}, \quad (8)$$

which completes the conversion. We note that such conversion process is probabilistic, since the state $|\Psi\rangle_{out}$ is obtained with a probability $p=50\%$, owing to the final polarizing step. Moreover, since we are using the $\{|H\rangle,|V\rangle\}$ basis for the polarization encoding and the $\{|+2\rangle,|-2\rangle\}=\{|l\rangle,|r\rangle\}$ for the OAM one, the transfer is associated also with a rotation of the Poincaré sphere. The correspondence of the six orthogonal states on the polarization Poincaré sphere with the six final ones in the OAM sphere is given in Table 1.

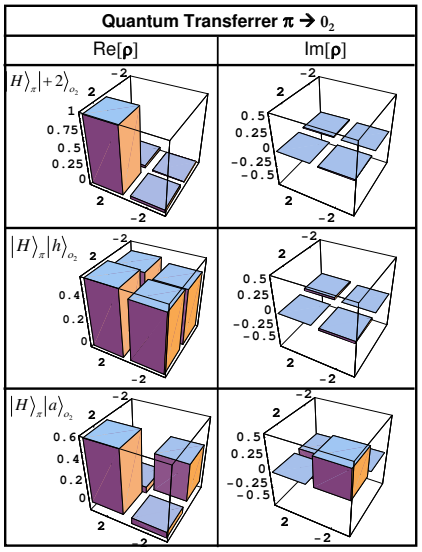

FIG. 4: Experimental density matrices ρ (the left column shows the real part and right column the imaginary part) measured for the output of the $\pi\rightarrow o_2$ qubit transfer, for each of the three different predicted output states shown in the upper left corner of each row.

The experimental layout of this scheme is shown in Fig. 2, dashed box **a**. The input arbitrary qubit is written in the polarization using two waveplates, as discussed in Sec. III. The final state tomography has been realized by means of the six holograms shown in Fig. 3 (left box). The experimental results for three specific choices of the input state are shown in Fig. 4. We find a good agreement with theory as demonstrated by the fidelity

Initial state	Final state	Fidelity
$\|H\rangle_\pi$	$\|+2\rangle=\|l\rangle_{o_2}$	(0.990 ± 0.002)
$\|V\rangle_\pi$	$\|-2\rangle=\|r\rangle_{o_2}$	(0.972 ± 0.002)
$\|A\rangle_\pi$	$\|h\rangle_{o_2}$	(0.981 ± 0.002)
$\|D\rangle_\pi$	$\|v\rangle_{o_2}$	(0.968 ± 0.002)
$\|L\rangle_\pi$	$\|a\rangle_{o_2}$	(0.998 ± 0.002)
$\|R\rangle_\pi$	$\|d\rangle_{o_2}$	(0.982 ± 0.002)

TABLE I: Fidelity values between the experimental states generated by the $\pi\rightarrow o_2$ transferrer and the theoretical ones expected after the conversion in the OAM degree of freedom of the qubit initially encoded in the polarization.

parameter, defined as $F=\langle\psi|\rho_{exp}|\psi\rangle$, where $|\psi\rangle$ is the theoretical state to be compared to the experimental one. Hence in this experiment the average fidelity value between the experimental states and the theoretical predictions is $F=(97.7\pm0.2)\%$. The fidelities obtained for six different input states are shown in Table 1.

Thus, we have demonstrated experimentally that the initial information encoded in an input TEM_{00} state can be coherently transferred to the OAM degree of freedom, thanks to the $\pi\rightarrow o_2$ converter, giving rise to the preparation of a qubit in the orbital angular momentum. As the initial information has been stored in the orbital part of the qubit wave-function, new information can be stored in the polarization degree of freedom, allowing the transportation in a single photon of a higher amount, at least two qubits, of information.

Transferrer OAM to polarization

Let us now show that the reverse process can be realized as well, by transferring a qubit initially encoded in the OAM subspace o_2 into the polarization space. We therefore consider as initial quantum state of the photon the following one:

$$|\Psi\rangle_{\mathrm{in}}=|H\rangle_\pi|\varphi\rangle_{o_2}=|H\rangle(\alpha|+2\rangle+\beta|-2\rangle) \quad (9)$$

By injecting the state $|\Psi\rangle_{in}$ in the q-plate device, and then rotating the output state by means of a pair of waveplates, we obtain the following state:

$$\frac{1}{2}\{\alpha|V\rangle|+4\rangle+\alpha|H\rangle|0\rangle+\beta|V\rangle|0\rangle+\beta|H\rangle|-4\rangle\} \quad (10)$$

Now, by coupling the beam to a single mode fiber, only the states with $m=0$ that is, the TEM_{00} modes, will be efficiently transmitted. Of course, this implies that a probabilistic process is obtained again, since we discard all the contributions with $m\neq0$ (ideally, again $p=50\%$). After the fiber, the output state reads:

$$|\Psi\rangle_{out}=(\alpha|H\rangle+\beta|V\rangle)|0\rangle=|\varphi\rangle_\pi|0\rangle_o \quad (11)$$

Initial state	Final state	Fidelity
$\|+2\rangle = \|l\rangle_{o_2}$	$\|H\rangle_\pi$	(0.981 ± 0.002)
$\|-2\rangle = \|r\rangle_{o_2}$	$\|V\rangle_\pi$	(0.995 ± 0.002)
$\|a\rangle_{o_2}$	$\|L\rangle_\pi$	(0.964 ± 0.002)
$\|d\rangle_{o_2}$	$\|R\rangle_\pi$	(0.972 ± 0.002)
$\|h\rangle_{o_2}$	$\|A\rangle_\pi$	(0.967 ± 0.002)
$\|v\rangle_{o_2}$	$\|D\rangle_\pi$	(0.970 ± 0.002)

TABLE II: Fidelity values between the experimental states generated by the $o_2 \rightarrow \pi$ transferrer and the theoretical ones expected after the conversion in polarization degree of freedom of the qubit initially encoded in the OAM.

which demonstrates the successful conversion from the OAM degree of freedom to the polarization one.

The experimental layout of this "reverse" scheme is shown in Fig. 2, dashed box **b**. The input qubit in OAM is prepared using one of the six holograms shown in Fig. 3 (left box), as explained in the previous Section. The output state is analyzed by a standard polarization-state quantum tomography. The experimental results for three cases are shown in Fig. 5. We find again a good agreement with theory, with an average fidelity $F = (97.3 \pm 0.2)\%$, and the specific cases shown in Table 2.

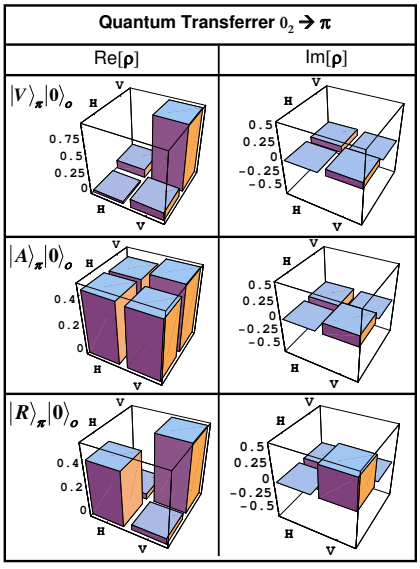

FIG. 5: Experimental density matrices ρ (the left column shows the real part and right column the imaginary part) measured for the output of the $o_2 \rightarrow \pi$ qubit transfer, for each of the three different predicted output states shown in the upper left corner of each row.

We note that this OAM-to-polarization transferrer allows a simple detection of the sign of the OAM, with a theoretical efficiency of 50%, much larger than what is typically obtained by the fork holograms ($10\% \div 30\%$). Therefore, this scheme can be used as a very efficient OAM detector.

Bidirectional transfer polarization-OAM-polarization

Having demonstrated polarization-to-OAM transfer and OAM-to-polarization transfer, it is natural to try both schemes together, in a bidirectional transfer which starts and ends with polarization encoding, with OAM as an intermediate state which can be used for example for communication. This is also the first quantum experiment based on the combined use of two q-plates. Although this test in principle is not involving any new idea with respect to the previous two experiments, it is important to verify that in practice the efficiency of the optical manipulation is not strongly affected by the number of q-plate employed, for example due to alignment criticality.

The layout is shown in Fig. 2, dashed box **c**, and corresponds to the sequence of the two schemes discussed above. In Fig. 6 we show some density matrices obtained by the quantum tomography technique in the polarization degree of freedom of the output state.

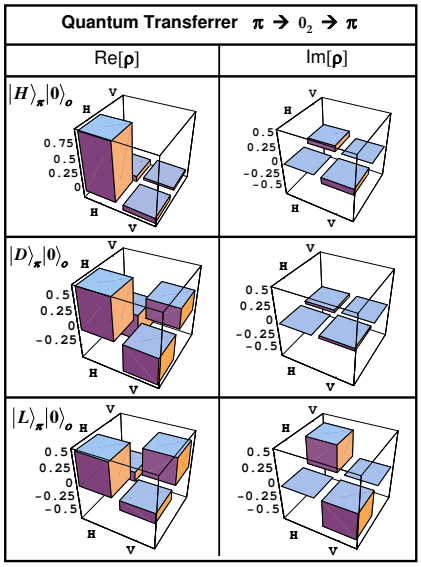

FIG. 6: Experimental density matrices measured in the polarization degree of freedom after the bidirectional $\pi \rightarrow o_2 \rightarrow \pi$ transferrer. In each box is reported the expression of the initial and final state, to be compared with the experimental one described by the density matrix.

Initial and final state	Fidelity
$\|H\rangle_\pi$	(0.970 ± 0.002)
$\|V\rangle_\pi$	(0.972 ± 0.002)
$\|A\rangle_\pi$	(0.958 ± 0.002)
$\|D\rangle_\pi$	(0.955 ± 0.002)
$\|R\rangle_\pi$	(0.934 ± 0.002)
$\|L\rangle_\pi$	(0.962 ± 0.002)

TABLE III: Fidelity values between the input and output states for the bidirectional $\pi \rightarrow o_2 \rightarrow \pi$ transferrer.

As can be observed in Table 3, the experimental results are in good agreement with the theoretical predictions, with a mean fidelity value equal to $F = (95.9 \pm 0.2)\%$. We see that the overall fidelity is still quite good, so that there seem to be no significant problem to the combined use of many q-plates in a cascaded configuration. After the two q-plates the quantum efficiency of the conversion process, defined as the capability to convert a TEM_{00} mode in a pure Laguerre-Gauss, is still around 80% (to optimize the efficiency, the q-plate birefringent retardations δ were tuned by mechanical pressure).

Deterministic conversion processes

The quantum transferrers implemented experimentally up to now are probabilistic processes, with 50% success probability. However, we now show that it is possible to realize a fully *deterministic* transferrer for both directions polarization-OAM and backward. This is obtained at the price of a slightly more complex optical layout, based on a q-plate and a Mach-Zehnder interferometer, shown in Fig. 7. The deterministic transferrer is bidirectional, and it converts the polarization in OAM ($\pi \rightarrow o_2$) if crossed in one way and the OAM in polarization ($o_2 \rightarrow \pi$) if crossed in the opposite way.

Let us consider first the $\pi \rightarrow o_2$ conversion. The initial state reads:

$$|\Psi\rangle_{in} = |\varphi\rangle_\pi |0\rangle_o = (\alpha|H\rangle + \beta|V\rangle)|0\rangle \qquad (12)$$

A pair of quarter waveplates converts it into the L, R basis, and then the QP is applied, so as to obtain the following state:

$$\alpha|R\rangle|+2\rangle + \beta|L\rangle|-2\rangle \qquad (13)$$

Another set of half-wave plates rotate the polarization basis in $|A\rangle, |D\rangle$, leading to $\alpha|A\rangle|+2\rangle + \beta|D\rangle|-2\rangle$:

$$\frac{1}{\sqrt{2}}\left(|H\rangle(\alpha|+2\rangle + \beta|-2\rangle) + |V\rangle(\alpha|+2\rangle - \beta|-2\rangle)\right) \qquad (14)$$

Such state is then injected in a PBS that separates the two linear polarizations and sends them in the two arms of a Mach-Zehnder interferometer. In one arm of the interferometer, say the V-polarized one, a device acting as a Pauli's operator $\tilde{\sigma}_z$ is inserted that operates only on the OAM states. This operator can be for example realized by means of a Dove's prism rotated at a $\pi/8$ angle in the lab frame followed by another Dove's prism rotated at zero angle, eventually with a set of compensating waveplates for correcting possible polarization variations. Alternatively, one Dove's prism can be put in one arm and the other in the other arm of the interferometer (to make it more balanced), both rotated by $\pi/16$. At each reflection in a mirror or in the PBS (as well as in a Dove's prism) the OAM is flipped ($m \rightarrow -m$). However, the overall number of reflections is even in both paths, so we can ignore this effect (however, some care must be taken for computing the correct phases of each term).

Mathematically, the $\tilde{\sigma}_z$ device will just change sign to the last term in Eq. (15). Therefore, the state in the interferometer becomes the following:

$$|H\rangle\frac{1}{\sqrt{2}}(\alpha|+2\rangle + \beta|-2\rangle) + |V\rangle\frac{1}{\sqrt{2}}(\alpha|+2\rangle + \beta|-2\rangle) \qquad (15)$$

where it is understood that $|H\rangle$ is also associated with one arm and $|V\rangle$ with the other arm of the interferometer. After the exit PBS, these two states are again superimposed in the same mode and provide only a single output on one exit face of the PBS, which is the following:

$$|A\rangle(\alpha|+2\rangle + \beta|-2\rangle) \qquad (16)$$

The polarization state is then finally rotated to H by a final half-wave plate rotated by 22.5°. Thus, the expected final state

$$|\Psi\rangle_{out} = |H\rangle(\alpha|+2\rangle + \beta|-2\rangle) = |H\rangle_\pi|\varphi\rangle_{o_2} \qquad (17)$$

is obtained, this time deterministically, as no contribution has been discarded [24]. The opposite conversion, $o_2 \rightarrow \pi$, is obtained by simply reversing the direction of light propagation in the same setup. All the transformations are then reversed and provide the desired information transfer from OAM to polarization, again fully deterministically.

MANIPULATION OF ORBITAL ANGULAR MOMENTUM IN THE SUBSPACE $|m| = 4$

In the bidirectional transfer, we have experimentally demonstrated that it is possible to work with two sequential q-plates without a significant lowering of the overall efficiency. This approach can be also adopted to access higher-order subspaces of the orbital angular momentum, by moving from one subspace to the next using a sequence of QPs alternated with half-wave plates [17].

Experimentally we have studied the case of two sequential q-plates QP_1 and QP_2 (both with $q = 1$). We demonstrate that it is possible to efficiently encode the quantum

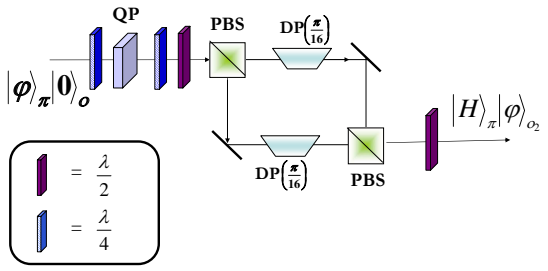

FIG. 7: Schematic representation of deterministic transferrer: A pair of suitably rotated Dove's prisms (DP), combined with wave plates for polarization compensation, are used to realize a $sigma_z$ operation on the OAM degree of freedom. The transferrer converts the polarization in OAM if the light goes from left to right, while it converts the OAM into polarization if crossed from right to left.

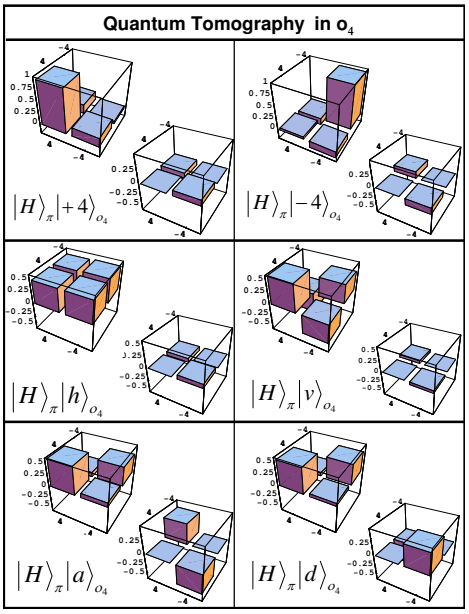

FIG. 8: Experimental density matrices measured in the OAM basis $\{|+4\rangle, |-4\rangle\}$ for different predicted final states, shown in the lower-left corner of each panel.

Initial state	Final state	Fidelity
$\|H\rangle_\pi$	$\|+4\rangle = \|l\rangle_{o_4}$	(0.947 ± 0.002)
$\|V\rangle_\pi$	$\|-4\rangle = \|r\rangle_{o_4}$	(0.958 ± 0.002)
$\|L\rangle_\pi$	$\|a\rangle_{o_4}$	(0.992 ± 0.002)
$\|R\rangle_\pi$	$\|d\rangle_{o_4}$	(0.923 ± 0.002)
$\|A\rangle_\pi$	$\|h\rangle_{o_4}$	(0.994 ± 0.002)
$\|D\rangle_\pi$	$\|v\rangle_{o_4}$	(0.955 ± 0.002)

TABLE IV: Fidelity values between the expected and the experimental states generated by the $\pi \to o_4$ transferrer.

information in the OAM basis $\{|+4\rangle, |-4\rangle\}$, by exploiting the spin-orbit coupling in the q-plates. In order to analyze the orbital angular momentum with $|m| = 4$ we have adopted newly designed holograms, shown in Fig. 3 (box on the right).

An initial state in the TEM_{00} mode and arbitrary polarization $|\varphi\rangle_\pi = (\alpha|H\rangle + \beta|V\rangle)$ is transformed by a pair of quarter-wave plates and QP_1 into the following one:

$$|\varphi\rangle_\pi|0\rangle_l \to (\alpha|R\rangle|-2\rangle + \beta|L\rangle|+2\rangle) \qquad (18)$$

A half-wave plate then inverts the polarization of the output state after QP_1, so that we get:

$$\alpha|L\rangle|+2\rangle + \beta|R\rangle|-2\rangle \qquad (19)$$

Next, the action of QP_2 and a polarizer leads to the final state:

$$(\alpha|+4\rangle + \beta|-4\rangle)|H\rangle = |\varphi\rangle_{o_4}|H\rangle_\pi \qquad (20)$$

By changing the different hologram masks, we have carried out the quantum state tomography reported in Fig. 8. The fidelity related to each state is reported in Table 4, and the high accordance between theory and experimental data leads to an average value $F = (96.1 \pm 0.2)\%$.

CONCLUSION

In this work we have demonstrated several optical schemes for the efficient quantum manipulation of the orbital angular momentum degree of freedom of single photons. All these schemes are based on the q-plate, a novel optical device that introduces a coupling between the polarization and the orbital angular momentum. We have experimentally demonstrated the coherent transfer of a qubit from the polarization to the orbital angular momentum and vice versa. We have also demonstrated the scalability of this approach, by cascading two q-plates in order to accomplish (i) the bidirectional transfer from the polarization to the orbital angular momentum and back to polarization and (ii) access to higher orders of orbital angular momentum. In all these demonstrations we achieved very good fidelities, as calculated by quantum tomographies of the resulting qubits, and also good quantum efficiencies. The schemes demonstrated experi-

mentally are probabilistic, with 50% success rate. However, we have also proposed a related scheme that is fully deterministic, although slightly more complex.

These results simplify the use of orbital angular momentum for encoding the quantum information in a single photon and can make its manipulation more convenient, by linking this orbital degree of freedom to the standard one of polarization. In perspective, this approach would allow realizing simple and effective schemes for higher dimensional quantum information processing and communication with photons.

* Electronic address: fabio.sciarrino@uniroma1.it

[1] L. Allen, M. W. Beijersbergen, R. J. C. Spreeuw, J. P. Woederman, Phys. Rev. A **45**, 8185 (1992).

[2] G. Molina-Terriza, J. P. Torres, L. and Torner, Nature Physics **3**, 305 (2007).

[3] A. Mair, A. Vaziri, G. Weihs, and A. Zeilinger, Nature(London) **412**, 313 (2001).

[4] G. Molina-Terriza, J. P. Torres, and L. Torner, Opt. Comm. **228**, 115 (2003).

[5] A. Vaziri, J. W. Pan, T. Jennewein, G. Weihs, and A. Zeilinger, Phys. Rev. Lett. **91**, 227902 (2003).

[6] H. Arnaut, and G. A. Barbosa, Phys. rev. Lett., **85**, 286-289 (2000)

[7] S. Franke-Arnold, S. M. Barnett, M. J. Padgett and L. Allen, Phys. Rev. A **65**, 033823 (2002)

[8] M. Sttz, S. Grblacher, T. Jennewein, A. Zeilinger, Appl. Phys. Lett. **90**, 261114 (2007).

[9] N. K. Langford, R. B. Dalton, M. D. Harvey, J. L. O'Brien, G. J. Pryde, A. Gilchrist, S. D. Bartlett, and A. G. White, Phys. Rev. Lett. **93**, 053601 (2004).

[10] A. Vaziri, G. Weihs, and A. Zeilinger, Phys. Rev. Lett. **89**, 240401 (2002)

[11] A. Aiello, S. S. R. Oemrawsingh, E. R. Eliel, and J. P. Woerdman, Phys. Rev. A **72**, 052114 (2005); S. S. Oemrawsingh, X. Ma, D. Voigt, A. Aiello, E. R. Eliel, G. W. t Hooft, and J. P. Woerdman Phys. Rev. Lett. **95**, 240501 (2005); S. S. Oemrawsingh, J. A. de Jong, X. Ma, A. Aiello, E. R. Eliel, G. W. t Hooft, and J. P. Woerdman, Phys. Rev. A **73**, 032339 (2006); J. B. Pors, A. Aiello, S. S. R. Oemrawsingh, M. P. van Exter, E. R. Eliel, and J. P. Woerdman Phys. Rev. A **77**, 033845 (2008).

[12] J. T. Barreiro, N. K. Langford, N. A. Peters, and P.G. Kwiat, Phys. Rev. Lett. **95**, 260501 (2005).

[13] J. T. Barreiro, T. C. Wei, and P. G. Kwiat, Nature Physics **4**, 282 (2008).

[14] L. Marrucci, C. Manzo, D. and Paparo, Phys. Rev. Lett. **96**, 163905 (2006).

[15] E. Nagali, F. Sciarrino, F. De Martini, L. Marrucci, B. Piccirillo, E. Karimi and E. Santamato, quant-phys arXiv:0810.2417 (2008).

[16] J. B. Gotte, et al., Opt. Express **16**, 993-1006 (2008)

[17] L. Marrucci, C. Manzo, and D. Paparo, Appl. Phys. Lett. **88**, 221102 (2006).

[18] M. Stalder, and M. Schadt, Optics Letters **21**, 1948 (1996)

[19] G. F. Calvo, et al., *Opt. Lett.* **32**, 7 (2007)

[20] E. Karimi, B. Piccirillo, L. Marrucci, and E. Santamato, arXiv:0809.4220 (2008).

[21] E. Karimi, G. Zito, B. Piccirillo, L. Marrucci, and E. Santamato, *Optics Letters*, **32**, 21, 3053-3055 (2007)

[22] P.G. Kwiat, K. Mattle, H. Weinfurter, A. Zeilinger, A.V. Sergienko, and Y.H. Shih, Phys. Rev. Lett. **75**, 4337 (1995).

[23] M.J. Padgett, and J. Courtial, Opt. Lett., **24**, 430 (1999).

[24] We note that, although the optical layout is a Mach-Zehnder interferometer, the optical path phase difference between the two arms of the interferometer is only affecting the polarization state of the single output obtained after the final PBS, while it does not act on the PBS exit mode and on the OAM final state. The final polarization may therefore turn elliptical if this phase difference is not well controlled. However, the H polarization can be easily restored by suitable wave-plates, as long as it is uniform. Therefore, this setup is expected to be relatively robust against misalignment.